

The ATESP radio survey

III. Source counts

I. Prandoni^{1,2}, L. Gregorini^{3,2}, P. Parma², H.R. de Ruiter^{4,2}, G. Vettolani², M.H. Wieringa⁵, and R.D. Ekers⁵

¹ Dipartimento di Astronomia, Università di Bologna, via Ranzani 1, I-40126, Bologna, Italy

² Istituto di Radioastronomia, CNR, Via Gobetti 101, I-40129, Bologna, Italy

³ Dipartimento di Fisica, Università di Bologna, Via Irnerio 46, I-40126, Bologna, Italy

⁴ Osservatorio Astronomico di Bologna, Via Ranzani 1, I-40126, Bologna, Italy

⁵ Australia Telescope National Facility, CSIRO, P.O. Box 76, Epping, NSW2121, Australia

Received 04 August 2000 / Accepted 16 October 2000

Abstract. This paper is part of a series reporting the results of the ATESP radio survey obtained at 1.4 GHz with the Australia Telescope Compact Array. The survey consists of 16 radio mosaics with $\sim 8'' \times 14''$ resolution and uniform sensitivity (1σ noise level $\sim 79 \mu\text{Jy}$) over the whole area of the ESO Slice Project redshift survey (~ 26 sq. degrees at $\delta \sim -40^\circ$). The ATESP survey has produced a catalogue of 2960 radio sources down to a flux limit (6σ) of ~ 0.5 mJy.

In this paper we present the 1.4 GHz $\log N - \log S$ relation derived from the ATESP radio source catalogue. The possible causes of incompleteness at the faint end of the source counts are extensively discussed and their effects are quantified and corrected for. The ATESP counts are consistent with others reported in the literature, even though some significant discrepancies are present at low fluxes (below a few mJy). We investigate whether such discrepancies may be explained in terms of field-to-field anisotropies, considering the fact that all the existing sub-mJy surveys cover small areas of sky (from a fraction of square degree to a few square degrees). We stress that the ATESP survey, covering 26 sq. degrees, provides the best determination of source counts available today in the flux range $0.7 \lesssim S_{1.4 \text{ GHz}} \lesssim 2$ mJy.

Key words. surveys – radio continuum: galaxies – galaxies: evolution

1. Introduction

The statistical study of radio sources allows us to address a number of astrophysical and cosmological problems, ranging from the evolution of classical radio galaxies and quasars to the properties of starburst galaxies as a function of cosmic time. The radio source counts are the most immediate product which can be derived from a radio survey and reflect the statistical properties of the radio source populations. The slope of the counts is determined essentially by the relative contribution of different types of sources at every flux, which is the result of their luminosity functions at various redshifts. The source counts therefore represent the most immediate observational constraint to evolutionary models of radio sources. An accurate determination of the source counts, their slope and normalization, is however necessary in order to make this constraint really useful. The source counts, together with measured local radio luminosity functions, can then be used to make predictions (about the redshift distribution, for instance) which can be verified once an extensive program of optical identification and spectroscopy has been completed in

some specific flux range.

Normalized differential source counts derived from deep 1.4 GHz surveys show a flattening below a few mJy. This change in slope is usually interpreted as the result of the emergence of a new population which does not appear at higher flux densities, where the counts are dominated by the classical powerful radio galaxies and quasars (99% above 60 mJy, Windhorst et al. 1990). This new population is thought to be a mixture of several different types of objects (faint AGNs, normal spirals and ellipticals, starburst galaxies, etc.) whose relative importance changes as a function of the flux itself. Unfortunately the existing samples of faint radio sources are confined to regions of relatively small angular sizes and no complete optical follow-up of such samples has been carried out yet (see e.g. Gregorini & Prandoni 2000 for a review). It follows that conclusions about the composition of the faint radio sources are based on small and only partially identified samples, biased by the fact that only the brightest optical counterparts have spectral information. Many questions are therefore still open about the true nature and evolution of the faint radio source population and very little is known about the luminosity properties and redshift distribution of such sources.

The ATESP 1.4 GHz survey (Prandoni et al. 2000a, paper

I) - carried out with the Australia Telescope Compact Array in the past years - consists of 16 radio mosaics with $\sim 8'' \times 14''$ resolution and uniform sensitivity (1σ noise level ranging from $69 \mu\text{Jy}$ to $88 \mu\text{Jy}$ depending on the radio mosaic) covering a narrow strip of $26^\circ \times 1^\circ$ at $\delta \sim -40^\circ$. The ATESP survey has produced a catalogue of 3172 radio components, corresponding to 2960 distinct radio sources, down to a flux limit (6σ) of $\sim 0.5 \text{ mJy}$ (Prandoni et al. 2000b, Paper II). The ATESP sample represents the largest sample (26 sq. degr.) sensitive to sub-mJy fluxes available so far. It offers a unique opportunity to investigate the nature and evolution of the mJy and sub-mJy populations and provides a very accurate determination of the radio source counts down to sub-mJy fluxes (the most accurate in the range $0.7 - 2 \text{ mJy}$). In this respect the ATESP survey fully complements the FIRST (White et al. 1997), which provides the most accurate determination of the source counts between 2 and 30 mJy.

This paper is organized as follows. The catalogue completeness is discussed in Sect. 2. The ATESP number counts are derived in Sect. 3 and the possible effect of clustering on the faint end of the counts is discussed in Sect. 4. Results are summarized in Sect. 5.

2. Catalogue Completeness

The detection of a source depends on the ratio of the *measured* peak flux density¹ over the *local* noise level. In order to use the ATESP source catalogue for statistical purposes (like the derivation of the source number counts), the possible causes of incompleteness in the catalogue have to be recognized and taken into account.

2.1. Visibility Area

Radio mosaics usually have a varying sensitivity over the region surveyed. This means that the area over which a source can be detected (visibility area, Katgert et al. 1973) increases with the source peak flux. The ATESP survey is characterized by a noise distribution which is fairly uniform within each mosaic and from mosaic to mosaic ($< 10\%$ variations). Average mosaic noise values vary from $\sim 69 \mu\text{Jy}$ to $\sim 88 \mu\text{Jy}$ (see Table B1 in paper II) with an average value of $\sim 79 \mu\text{Jy}$ (1σ). Also, the noise can generally be considered Gaussian, with only a few exceptions around strong sources ($S_{\text{peak}} > 50 - 100 \text{ mJy}$) where higher noise levels ($\sim 100 \mu\text{Jy}$) can be occasionally found (see Paper I and II for more details).

The visibility area of the ATESP survey is shown in Fig. 1. As expected, the fraction of the total area over which an ATESP source of a given peak flux density can be detected, increases very rapidly between 0.4 and 0.5 mJy and becomes equal to 1 at $S_{\text{peak}} \geq 0.8 \text{ mJy}$. This is a consequence of the ATESP observing strategy (uniform sensitivity in the whole region surveyed) and of the fact that high noise regions around bright sources do not affect the source detection above 0.8 mJy.

¹ Peak flux density is always intended as brightness in units of mJy per beam solid angle.

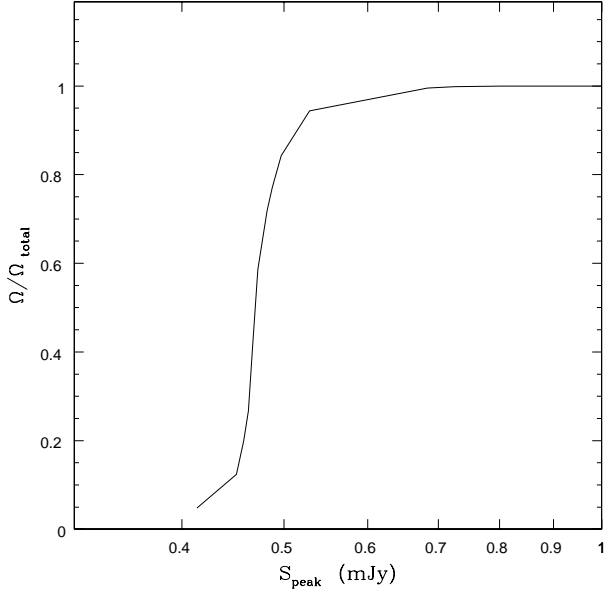


Fig. 1. Visibility area of the ATESP survey. Fraction of the total area over which a source with given measured peak flux density can be detected (i.e. $S_{\text{peak}}^{\text{meas}} \geq 6\sigma$).

2.2. Systematic Effects

Two additional effects could be responsible of partial incompleteness at low signal-to-noise ratios: the clean bias and the bandwidth smearing. The clean bias has been extensively discussed in paper I of this series. It is responsible for both total and peak flux density under-estimations of the order of 10–20% at the lowest flux levels ($S_{\text{peak}} < 10\sigma$) and gradually disappears going to higher fluxes (no effect for $S_{\text{peak}} \geq 50 - 100\sigma$). The bandwidth smearing, extensively discussed in paper II, could allow for an extra 5% under-estimation of the peak flux densities only.

In paper II (Appendix B) we gave a formula (Eq. (B1)) to correct the measured (peak and total) fluxes for the clean bias and bandwidth smearing. Such a correction varies from source to source depending on the radio mosaic and on the source signal-to-noise ratio. However, peak flux densities are *at most* underestimated by a factor of $\sim 25\%$ due to the combined effects of clean bias and smearing (see paper I and II). It follows that *at most* $S_{\text{peak}}^{\text{meas}} \sim 0.75 S_{\text{peak}}^{\text{corr}}$. This means that any source with *corrected* peak flux density $\gtrsim 6\sigma/0.75$ will have effective *measured* peak flux densities still above the detection threshold of the ATESP survey. In other words, incompleteness due to clean bias and bandwidth smearing does not affect the ATESP catalogue at *corrected* peak fluxes $> 0.55 - 0.70 \text{ mJy}$, the precise value depending on the radio mosaic.

2.3. Resolution Bias

In deriving the source number counts, the completeness of the catalogue in terms of total flux density is very important. Such a completeness depends on the source angular size and its com-

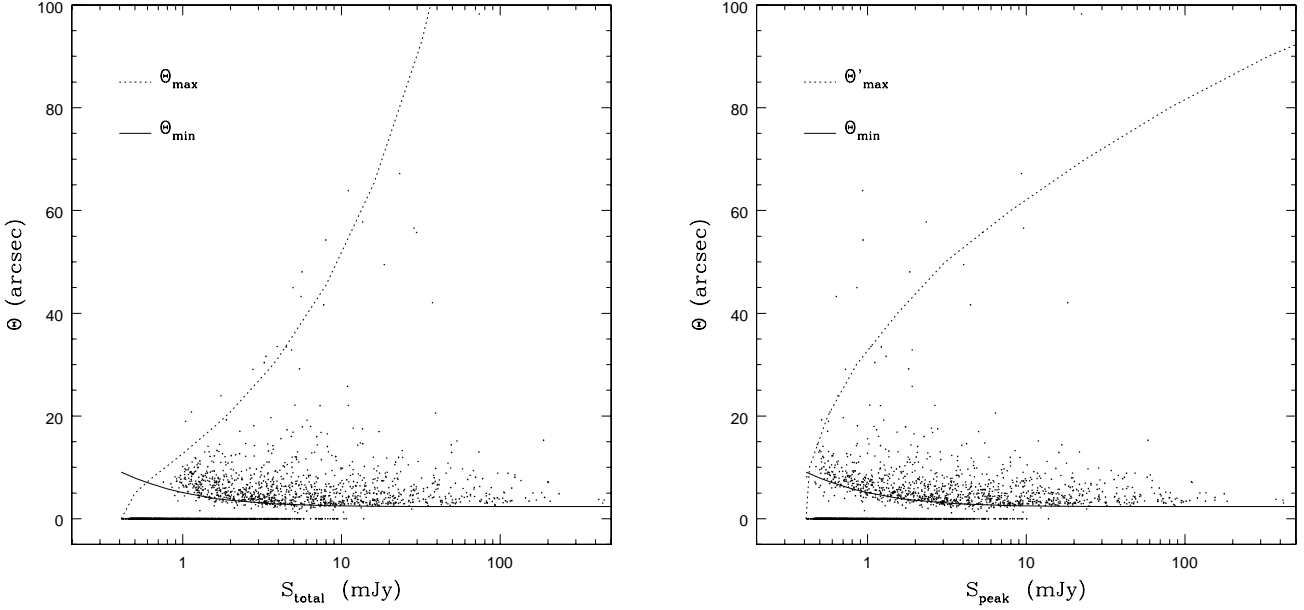


Fig. 2. Left Panel. Angular size (geometric mean after deconvolution) for the 3172 ATESP radio components as a function of the measured *total* flux density. The maximum size (Θ_{\max}) that a source of a given $S_{\text{total}}^{\text{meas}}$ can have before dropping below the limiting flux of the survey is indicated by the dotted line. Also indicated is the minimum angular size (Θ_{\min}), below which deconvolution is not considered significant (solid line). The lines are drawn assuming for the survey a 6σ limit of 0.41 mJy, obtained assuming the lowest average noise value measured in the ATESP radio mosaics (i.e. $\sigma = 69 \mu\text{Jy}$, see Table B1 in paper II). All unresolved sources are indicated in the figure by dots at $\Theta = 0$. **Right Panel.** Same as in the left panel but as a function of the measured *peak* flux density. Here the dotted line indicates the maximum scale (Θ'_{\max}) at which the ATESP survey is sensitive due to the lack of baselines shorter than 500 m, while the solid line still indicates the minimum angular size (Θ_{\min}), below which deconvolution is not considered significant.

ponent flux ratio. A resolved source of given S_{total} will drop below the 6σ peak flux density cut-off more easily than a point source of same S_{total} . This is the so-called resolution bias.

Eq. (1) of Paper II can be used to give an approximate estimate of the maximum size (Θ_{\max}) a source of given S_{total} can have before dropping below the 6σ limit of the ATESP catalogue. In Fig. 2 (left panel) we plot the angular size (Θ) of the ATESP radio sources (or source components) as a function of the measured total flux density. Θ is defined as the geometric mean of the (Gaussian) major and minor deconvolved axes of the ATESP sources as listed in the ATESP catalogue (see Paper II). We notice that for unresolved sources (dots at $\Theta = 0$) we assume $S_{\text{total}} = S_{\text{peak}}$. As expected, the angular sizes of the largest ATESP sources are in good agreement with the estimated Θ_{\max} (dotted line).

The $\Theta_{\max} - S_{\text{total}}$ constraint is complemented by a second one which is a function of the peak flux and takes into account, through the so-called visibility function, the maximum scale at which the ATESP survey is sensitive due to the lack of baselines shorter than 500 m (see paper I, Sect. 4, for more details). This latter constraint (Θ'_{\max}) is indicated by the dotted line in the right panel of Fig. 2 and, as expected, follows the angular size distribution of the largest ATESP sources as a function of their measured peak fluxes. The $\Theta'_{\max} - S_{\text{peak}}$ relation is important at high fluxes ($\gtrsim 20$ mJy), where it provides a more

stringent constraint than the $\Theta_{\max} - S_{\text{total}}$ relation.

A third constraint on source angular sizes should be considered when dealing with resolution incompleteness effects. As discussed in Paper II, the deconvolution efficiency depends on the size of the ATESP survey synthesized beam ($\sim 8'' \times 14''$) and increases with the source signal-to-noise ratio: at the lowest peak flux levels only sources with $\Theta \gtrsim 8'' - 10''$ are reliably resolved; on the contrary, at the highest peak flux densities, sources with angular sizes as small as $\Theta \sim 2''$ can be resolved. Eqs. (1) and (2) of Paper II can be used to derive an approximate estimate of the minimum angular size (Θ_{\min}) that is reliably resolved as a function of the source peak flux. Θ_{\min} is indicated by the solid lines in Fig. 2 (since $S_{\text{total}} = S_{\text{peak}}$ for unresolved sources, we have plotted it in both panels). The Θ_{\min} constraint is important at low flux levels where Θ_{\max} and Θ'_{\max} become both unphysical (i.e. $\rightarrow 0$).

The three constraints discussed above (Θ_{\max} , Θ'_{\max} and Θ_{\min}) have been used to define an overall angular size upper limit, Θ_{lim} , as a function of the ATESP source flux density:

$$\Theta_{\text{lim}} = \max[\Theta_{\min}, \min(\Theta_{\max}, \Theta'_{\max})]. \quad (1)$$

In order to estimate the incompleteness in the ATESP catalogue due to resolution bias, we need to make an assumption about the *true* angular size distribution of radio sources as a function of flux. Following Windhorst et al. (1990), we have as-

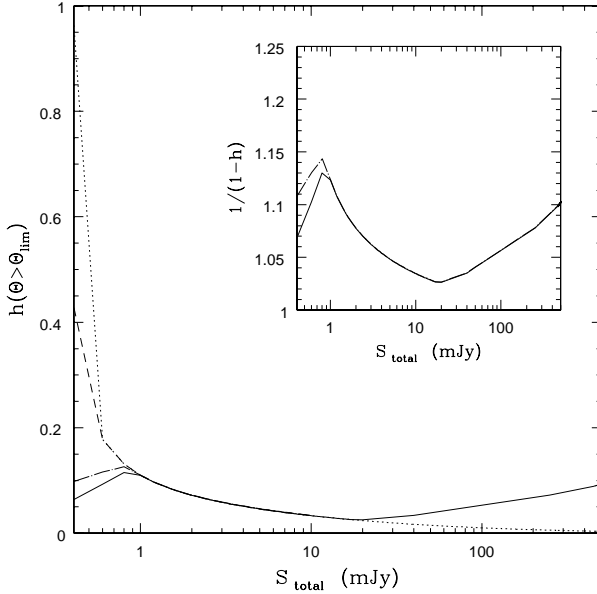


Fig. 3. Fraction of sources with angular size larger than Θ_{lim} ($h(> \Theta_{\text{lim}})$) as a function of the total source flux S_{total} (computed as proposed by Windhorst et al. 1990). Θ_{lim} represents the maximum size a source of given S_{total} can have in order to be detected in the ATESP survey. Different curves are found for different definitions of Θ_{lim} (see text): $\Theta_{\text{lim}} = \max[\Theta_{\text{min}}, \min(\Theta_{\text{max}}, \Theta'_{\text{max}})]$ (solid line); $\Theta_{\text{lim}} = \max[2'', \min(\Theta_{\text{max}}, \Theta'_{\text{max}})]$ (dashed line); $\Theta_{\text{lim}} = \Theta_{\text{max}}$ (dotted line). Also shown is the curve obtained by assuming $\Theta_{\text{med}} = 2''$ for sub-mJy sources, as discussed in the text (dot-dashed line). The inner panel shows the effect of the two different definitions of Θ_{med} on the form of the resolution bias correction to be applied to the source counts.

sumed $h(> \Theta_{\text{lim}}) = e^{-\ln 2 (\Theta_{\text{lim}}/\Theta_{\text{med}})^{0.62}}$ and $\Theta_{\text{med}} = 2'' \cdot S_{1.4\text{GHz}}^{0.30}$ (S in mJy). Θ_{med} represents the estimated source median angular size at a given flux density. The Windhorst et al. equations together with Eq. (1) allowed us to estimate the fraction of sources of given S_{total} with angular sizes larger than Θ_{lim} and thus lost by the ATESP survey (solid line in Fig. 3). The rising slope of the curve at high flux densities is due to the constraint provided by Θ'_{max} . On the other hand, the decreasing trend at low fluxes is a consequence of the looser constraint provided by Θ_{min} . In fact, introducing Θ_{min} in the equation takes into account the effect of having a finite synthesized beam size (that is $\Theta_{\text{lim}} \gg 0$ at the survey limit) and a deconvolution efficiency which varies with the source peak flux.

In determining the resolution bias effect, a correct definition of Θ_{lim} is very important. The dashed and the dotted curves in Fig. 3 demonstrate how critical is the determination of the resolution bias effect at low signal-to-noise ratios. Slightly changing the definition of Θ_{lim} can in fact produce very different results. The dashed line shows the effect on $h(> \Theta_{\text{lim}})$ when a fixed value for Θ_{min} in Eq. (1) is assumed. In this case Θ_{min} was set equal to $2''$, that is the minimum angular size that is reliably deconvolved at the highest flux densities, in the

case of the ATESP survey. The dotted line shows, on the contrary, the effect of letting $\Theta_{\text{lim}} \rightarrow 0$ for $S \rightarrow 6\sigma$, by defining $\Theta_{\text{lim}} = \Theta_{\text{max}}$ (we also neglect the effect of Θ'_{max}). The fraction of lost sources will approach 1 at the survey limit (dotted line), while it monotonically decreases going to higher fluxes.

We have also investigated the effect of assuming a constant value $\Theta_{\text{med}} = 2''$ for sources with $S \leq 1$ mJy, as suggested by recent studies (e.g. Windhorst et al. 1993, Richards 2000). The corresponding $h(> \Theta_{\text{lim}})$ is indicated by the dot-dashed line in Fig. 3. As shown in the figure, this more realistic assumption results in a larger fraction of lost sources at $S < 1$ mJy (10% instead of 6% at the survey limit). The uncertainty in the form of Θ_{med} at sub-mJy fluxes obviously translates in an uncertainty in the form of the resolution bias correction ($c = 1/[1 - h(> \Theta_{\text{lim}})]$) to be applied to the source counts (see inner panel of Fig. 3). At sub-mJy fluxes, this upward systematic uncertainty ($\leq 4\%$) has to be (quadratically) added to a more general 10% uncertainty in the resolution bias correction (as indicatively quantified by Windhorst et al. 1990).

3. The ATESP Source Counts

We used the 6σ ATESP catalogue (Paper II) to derive the differential ATESP source counts down to 0.41 mJy. In computing the counts we have used the integrated flux for extended sources and the peak flux for point-like sources. Each source has been weighted for the reciprocal of its visibility area ($\Omega(S_{\text{peak}})/\Omega_{\text{total}}$, see Fig. 1), that is the area over which the source could be detected. We notice that for $S_{\text{peak}} > 0.8$ mJy a source can be counted over the whole survey area.

In Fig. 4 we present the ATESP counts derived from the 3172 ATESP components (empty circles) and from the 2960 distinct radio sources defined from them, that is counting any multi-component source as one (filled circles). In this figure no corrections were applied to take into account either the systematic under-estimations of the flux densities (see Sect. 2.2) or the resolution bias (see Sect. 2.3). Horizontal bars represent 1σ errors in the measured flux ($\sigma(S^{\text{meas}})$), calculated as discussed in Paper II. Vertical bars represent Poissonian errors (calculated following Regener 1951).

In the ATESP catalogue a source is defined as *multiple* whenever two or more components are found closer than $45''$ (even though some exceptions are present, see Paper II for more details). Applying this distance constraint we expect $\sim 20\%$ contamination by random superpositions. Fig. 4 shows how possible spurious multiple sources could affect the ATESP source counts.

In Fig. 5 we show the effect of the flux and resolution bias corrections on the ATESP source counts (multiple sources are again counted as one). Filled circles and triangles indicate the counts respectively before and after correcting the flux densities for both the clean bias and the bandwidth smearing (fluxes are corrected as proposed in Paper II). In the latter case horizontal bars represent $\sigma(S^{\text{corr}})$, obtained by propagating the errors of the measured quantities S^{meas} , k , a and b which appear in Eq. (B1) of Paper II. We note that the plotted values of $\sigma(S^{\text{corr}})$ have to be considered as average estimates since they have been derived in the case of *intermediate* clean bias

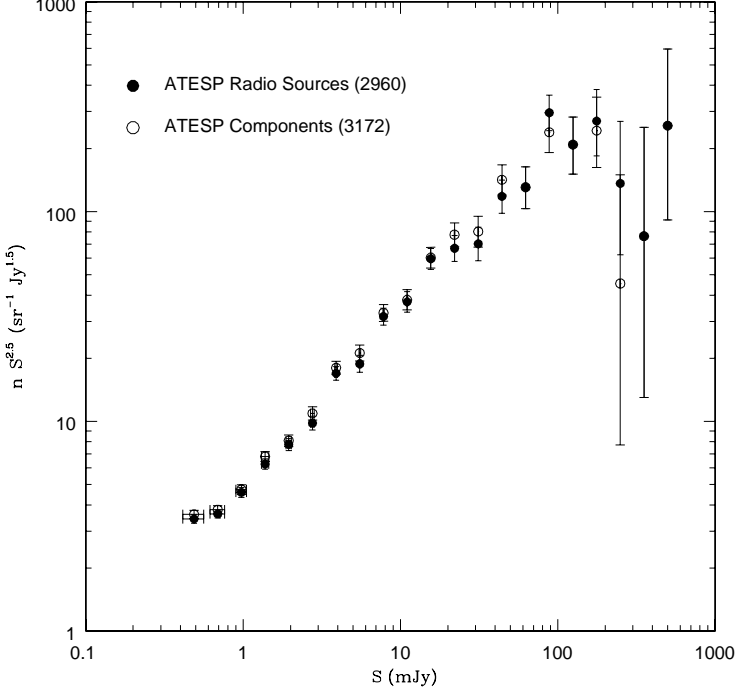


Fig. 4. Normalized 1.4 GHz differential source counts derived from the ATESP catalogue. Filled circles refer to the ATESP radio source catalogue (2960 distinct objects). Empty circles refer to the list of all the ATESP components (3172 entries). Horizontal bars represent 1σ errors in the *measured* total flux. Vertical bars represent Poissonian errors.

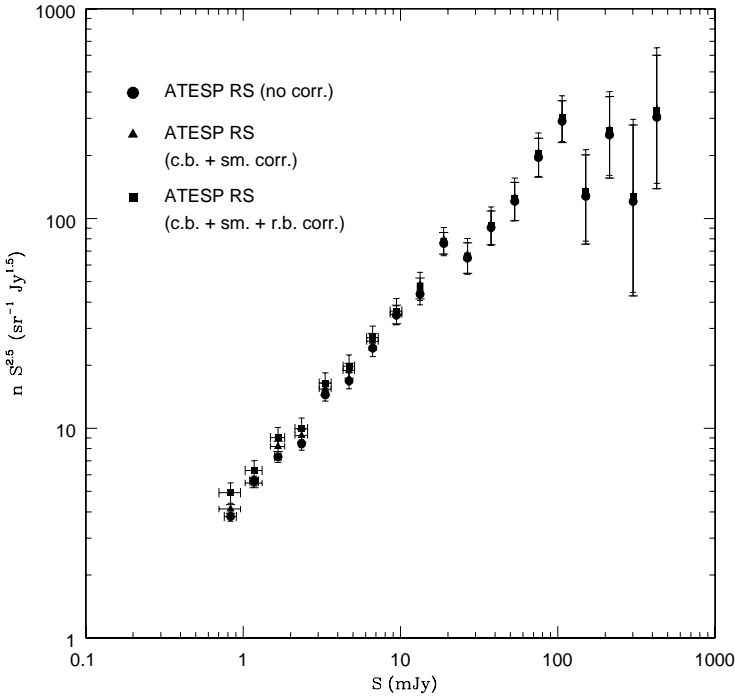


Fig. 5. Normalized 1.4 GHz differential source counts derived from the ATESP catalogue (multiple sources are counted as one object). The source counts are plotted before (filled circles, same as shown in Fig. 4) and after correcting for clean bias and bandwidth smearing (filled triangles). In the latter case horizontal bars represent 1σ errors in the *corrected* total flux. Filled squares represent the counts obtained once the resolution bias is also taken into account. Vertical bars include here the uncertainty in the resolution bias correction. In all cases the counts have been derived down to 0.70 mJy (instead of 0.41 mJy), in order to avoid the incompleteness effects introduced by the flux corrections.

correction parameters ($a = 0.13 \pm 0.03$ and $b = 0.75 \pm 0.06$, see discussion in Sect. 5.3 of Paper I). We also notice that $\sigma(k) = 0.006$. Filled squares in Fig. 5 show the effect of adding the resolution bias correction (computed following Windhorst et al. 1990, as discussed in Sect. 2.3). In the estimation of

the vertical bars we have here included the errors due to the uncertainty in the resolution bias correction (see Sect. 2.3). We notice that the ATESP counts presented in this figure are derived down to a limit of 0.70 mJy (instead of 0.41 mJy) in order to prevent the corrected counts to suffer from

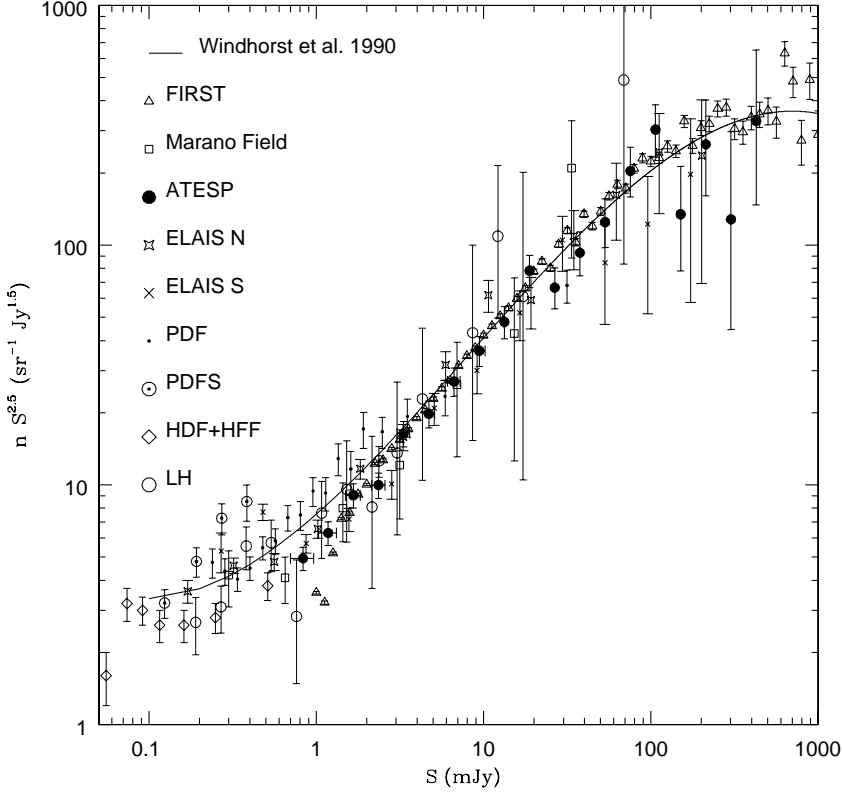


Fig. 6. Normalized 1.4 GHz differential source counts for different samples: the FIRST (triangles, White et al. 1997), the Marano Field (squares, Gruppioni et al. 1997), the ELAIS North and South (stars and crosses, Ciliegi et al. 1999 and Gruppioni et al. 1999), the Phoenix Deep Survey (dots and circled dots, Hopkins et al. 1998), the Hubble Deep Field + Flanking Fields (diamonds, Richards 2000) and the Lockman Hole (empty circles, de Ruiter et al. 1997). The fit obtained by Windhorst et al. (1990) is also shown (solid line). The ATESP source counts presented here (filled circles), are corrected for clean bias, bandwidth smearing and resolution bias (same as filled squares presented in Fig. 5). Horizontal bars associated to the ATESP counts represent 1σ errors in the *corrected* total flux, while vertical bars include the uncertainty in the resolution bias correction.

Table 1. ATESP source counts.

ΔS (mJy)	$\langle S \rangle$ (mJy)	N_S	$nS^{2.5}$ ($\text{sr}^{-1} \text{Jy}^{1.5}$)
0.70 – 0.99	0.83 ± 0.13	466	$4.94^{+0.56}_{-0.54}$
0.99 – 1.40	1.18 ± 0.15	372	$6.30^{+0.72}_{-0.71}$
1.40 – 1.98	1.66 ± 0.17	331	$9.05^{+1.05}_{-1.03}$
1.98 – 2.80	2.35 ± 0.22	222	$9.99^{+1.23}_{-1.20}$
2.80 – 3.96	3.33 ± 0.29	220	$16.4^{+2.0}_{-2.0}$
3.96 – 5.60	4.71 ± 0.40	160	$19.8^{+2.6}_{-2.5}$
5.60 – 7.92	6.66 ± 0.56	131	$27.0^{+3.7}_{-3.6}$
7.92 – 11.2	9.42 ± 0.80	105	$36.2^{+5.3}_{-5.1}$
11.2 – 15.8	13.3 ± 0.1	83	$47.8^{+7.5}_{-7.1}$
15.8 – 22.4	18.8 ± 0.1	81	$78.2^{+12.4}_{-11.7}$
22.4 – 31.7	26.6 ± 0.2	41	$66.5^{+13.7}_{-12.3}$
31.7 – 44.8	37.7 ± 0.2	34	$93.0^{+20.9}_{-18.5}$
44.8 – 63.4	53.3 ± 0.3	27	125^{+31}_{-27}
63.4 – 89.6	75.3 ± 0.4	26	204^{+52}_{-45}
89.6 – 127	107 ± 1	23	303^{+82}_{-70}
127 – 179	151 ± 1	6	134^{+78}_{-57}
179 – 253	213 ± 1	7	263^{+140}_{-103}
253 – 358	301 ± 2	2	128^{+170}_{-84}
358 – 507	426 ± 2	3	329^{+322}_{-182}

incompleteness (see discussion in Sect. 2).

The final ATESP source counts (those corrected for all the effects and indicated by filled squares in Fig. 5) are also listed in Table 1, where, for each flux interval (ΔS), the flux geometric mean ($\langle S \rangle$), the number of sources detected (N_S) and the weighted normalized differential counts ($nS^{2.5}$) are given. Also listed are the errors associated to ΔS and to the normalized counts (computed as discussed above). In this table fluxes are intended as total corrected flux densities. The final ATESP source counts have then been compared with the most updated previous determinations at 1.4 GHz (see Fig. 6). Also shown is the interpolation determined by Windhorst et al. (1990) from a collection of 10,575 radio sources belonging to 24 different surveys at 1.4 GHz, representing the state of the art at that time (solid line). As illustrated in Fig. 6 there is consistency between the ATESP counts and those obtained by other recent surveys, with the exception of the Phoenix Deep Survey (PDF and PDFS, Hopkins et al. 1998), whose counts at $S \geq 0.7$ mJy are systematically higher than the ATESP counts (and also higher than the counts derived from the other surveys presented in the figure).

We notice that according to the ATESP determination the upturn in the source counts should show up at lower fluxes ($S \lesssim 1$ mJy) than indicated by the Windhorst et al. (1990) fit ($S \lesssim 5$ mJy). The ATESP counts are in very good agreement with the FIRST counts (White et al. 1997, triangles in Fig. 6), which are the most accurate available today over the flux range 2–30 mJy. Our survey, on the other hand, provides the best determination of the counts at fainter fluxes ($0.7 < S < 2$ mJy), where

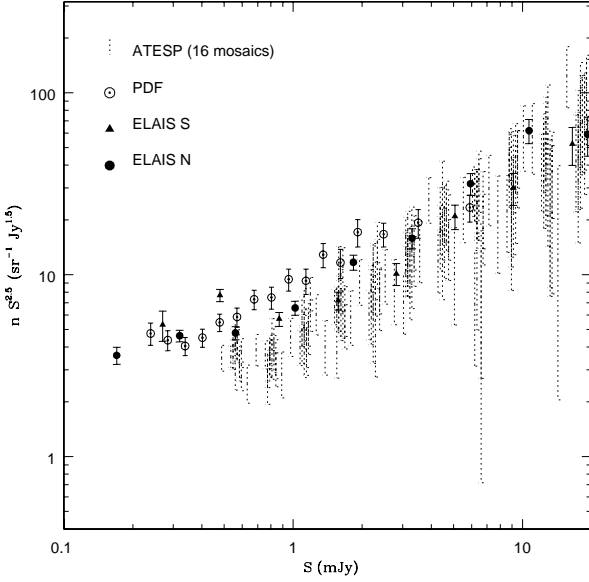


Fig. 7. Normalized 1.4 GHz differential source counts for the 16 ATESP mosaics separately (dotted 1σ Poissonian error bars). For consistency, these counts are compared only to the ones obtained from the surveys covering areas of the same order of magnitude (a few sq. degrees): the ELAIS North and South (filled circles and triangles) and the PDF (circled dots). The ATESP counts are not corrected for clean bias, bandwidth smearing and resolution bias (Horizontal error bars have not been drawn to prevent overcrowding).

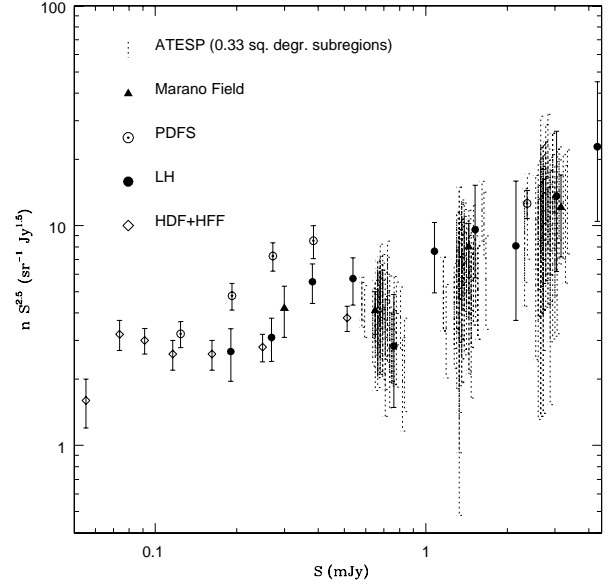


Fig. 8. Normalized 1.4 GHz differential source counts for 0.33 sq. degree ATESP sub-regions (dotted 1σ Poissonian error bars). For consistency these counts are compared only to the ones obtained from the surveys covering areas of the same order of magnitude (a fraction of sq. degree): the PDFS (circled dots), the Marano Field (triangles), the HDF+HFF (diamonds) and the Lockman Hole (filled circles). The ATESP counts are not corrected for clean bias, bandwidth smearing and resolution bias (Horizontal error bars have not been drawn to prevent overcrowding).

the FIRST becomes incomplete. The ATESP counts can thus provide an useful observational constraint on the evolutionary models for the mJy and sub-mJy populations.

Below a few mJy the number counts presented in Fig. 6 show a large spread. Such a spread can be due to technical reasons, like different corrections for resolution bias applied by different surveys (*e.g.* Hubble Deep Field, Phoenix Deep Survey, ATESP) or no correction at all (*e.g.* ELAIS, Marano Field). Note, however, that discrepancies are found even within the same survey: the deeper PDFS counts, for instance, are not consistent with the PDF counts in the overlapping flux range. This example suggests that the effect of field-to-field anisotropies and/or clustering could be very important, since the faintest samples typically cover very small regions of sky ($\ll 1$ sq. degree). This latter effect does not apply to the ATESP sample which covers 26 sq. degrees.

4. Clustering Effects on Deep Radio Counts

The ATESP survey allows us to test whether field-to-field anisotropies and/or clustering effects could explain, at least in part, the existing spread in source counts at low fluxes ($S \lesssim 1$ mJy). The largest sub-mJy surveys cover areas of the order of a few square degrees (typically 3 sq. degr.), while the deepest sub-mJy surveys cover only a fraction of square degree (typically 0.33 sq. degr.). We have therefore tested these two typi-

cal scales for sub-mJy radio surveys. The larger scale has been tested by deriving the counts for each of the 16 ATESP mosaics separately (mosaic areas range from 1.3 to 2 sq. degrees, see paper I). The smaller scale, on the other hand, has been tested by splitting the ATESP survey in $40' \times 30'$ (0.33 sq. degrees) sub-regions. Note that no correction for clean bias, bandwidth smearing and resolution bias has been applied in this analysis in order to derive the ATESP counts down to the detection limit of the survey (6σ) and to have a more meaningful comparison with the fainter surveys.

The results are reported in Figs. 7 and 8 (dotted error bars). For consistency, the ATESP counts obtained on these two scales have been compared only to surveys covering areas of the same order of magnitudes: the ELAIS and PDF for the larger scale (see Fig. 7) ; the MF, LH, PDFS and HDF+HFF for the smaller scale (see Fig. 8). In either case the ATESP counts are in good agreement with the ones derived from the comparison samples, at least down to the fluxes probed by the ATESP. This is particularly true if we consider that no corrections for clean bias, bandwidth smearing or resolution bias have been applied to the ATESP counts. It is therefore probable that field-to-field anisotropies do not play an important role in these samples. The only exception is represented by the PDF counts (circled dots in Fig. 7), which remain systematically in excess (in particular at fluxes $0.5 \lesssim S \lesssim 1$ mJy). On the other

hand, the excess shown by the PDFS counts (circled dots in Fig. 8) cannot be directly probed by the ATESP survey. From the analysis of Fig. 7 it seems very hard to explain the PDF counts in terms of Poissonian fluctuations. We have applied the Kolmogorov-Smirnov 2-sample test to the PDF and the ATESP counts shown in Fig. 7 (we have considered the counts derived from the 16 ATESP mosaics as a unique larger sample) and we found that the probability of the two samples being drawn from the same parent population is 0.2%. This leads us to conclude that either the PDF sample has a significant excess of sources or some other unknown systematic effect is present. It is however worth to notice that in general systematic discrepancies like the ones shown by the counts derived from the Phoenix Deep Survey cannot be explained in terms of different assumptions for resolution bias, because such an effect does strongly affect the counts only at low signal-to-noise ratios (see discussion in Sect. 2.3).

5. Summary

We have presented the $\log N - \log S$ relation derived from the ATESP catalogue. Particular emphasis has been given to the possible causes of incompleteness at the faint end of the source counts. In particular we have discussed the effect of systematic under-estimations in the measured flux densities due to clean bias and bandwidth smearing and we have quantified the incompleteness of the catalogue in terms of total flux density (the so-called resolution bias). Once corrected for such effects, the ATESP counts are consistent with the counts derived from other recent surveys. The only discrepant counts are those obtained from the Phoenix Deep Survey (Hopkins et al. 1998), which are systematically higher. It is worth to notice that the ATESP counts point towards lower fluxes ($S \lesssim 1$ mJy) for the upturn than those ($S \lesssim 5$ mJy) indicated by the Windhorst et al. (1990) best fit.

At fluxes below 1 mJy, the 1.4 GHz number counts derived from different surveys show a large spread. Such a spread can be due to technical reasons, like different corrections for resolution bias or no correction at all. The effect of field-to-field anisotropies and/or clustering could also play an important role, since the faintest samples typically cover very small regions of sky ($\ll 1$ sq. degree). This latter effect does not apply to the ATESP sample which covers 26 sq. degrees. We have investigated such a possibility by splitting the ATESP catalogue in smaller sub-samples. In particular we have tested two typical scales for sub-mJy radio surveys: a few sq. degrees for the largest surveys (1 – 2 sq. degr. in this case) and ~ 0.33 sq. degrees for the deepest surveys. As a result we have found that on both scales the spread in the counts can be simply explained in terms of Poissonian fluctuations, at least down to the flux densities probed by the ATESP. The only exception is represented by the Phoenix Deep Survey whose counts remain systematically higher than the ATESP counts. Such a discrepancy is statistically relevant and draws us to conclude that clustering and/or some other unknown systematic effect should play an important role in the case of the PDF sample.

The ATESP survey provides the best determination of the 1.4 GHz source counts in the flux range 0.7–2 mJy, and in this

respect it complements the FIRST (White et al. 1997) which provides the most accurate counts available at higher fluxes (2–30 mJy). The ATESP source counts can thus be used to set observational constraints on the evolutionary models for the mJy and sub-mJy populations.

Acknowledgements. The Australia Telescope is funded by the Commonwealth of Australia for operation as a National Facility managed by CSIRO. The authors acknowledge R. Fanti for reading and commenting on an earlier version of this manuscript.

References

- Cileigi P., McMahon R.G., Miley G., et al., 1999, MNRAS 302, 222
- de Ruiter H.R., Zamorani G., Parma P., et al., 1997, A&A 319, 7
- Gregorini L., Prandoni I. 2000, Mem. Soc. Astron. Ital. in press
- Gruppioni C., Zamorani G., de Ruiter H.R., et al., 1997, MNRAS 286, 470
- Gruppioni C., Cileigi P., Rowan-Robinson M., et al., 1999, MNRAS 305, 297
- Hopkins A.M., Mobasher B., Cram L., Rowan-Robinson M. 1998, MNRAS 296, 839
- Katgert P., Katgert-Merkelijn J.K., Le Poole R.S., van der Laan H. 1973, A&A 23, 171
- Prandoni I., Gregorini L., Parma P., et al., 2000a, A&AS 146, 31 (Paper I)
- Prandoni I., Gregorini L., Parma P., et al., 2000b, A&AS 146, 41 (Paper II)
- Regener V.H. 1951, Phys. Rev. Lett. 84, 161L
- Richards E.A. 2000, ApJ 533, 611
- White R.L., Becker R.H., Helfand D.J., Gregg M.D. 1997, ApJ 475, 479
- Windhorst R.A., Mathis D., Neuschaefer L. 1990. In: Kron R.G. (ed.) Evolution of the Universe of Galaxies, ASP Conf. Ser. 10, 389
- Windhorst R.A., Fomalont E.B., Partridge R.B., Lowenthal J.D. 1993, ApJ 405, 498